Proton and neutron correlations in ¹⁰B

AUTHOR(S):

Kanada-En'yo, Yoshiko; Morita, Hiroyuki; Kobayashi, Fumiharu

PHYSICAL REVIEW C **91**, 054323 (2015)

Proton and neutron correlations in ^{10}B

Yoshiko Kanada-En'yo and Hiroyuki Morita
Department of Physics, Kyoto University, Kyoto 606-8502, Japan

Fumiharu Kobayashi
Department of Physics, Niigata University, Niigata 950-2181, Japan

(Received 10 April 2015; published 26 May 2015)

We investigate positive-parity states of ^{10}B with the calculation of antisymmetrized molecular dynamics focusing on *pn* pair correlations. We discuss effects of the spin-orbit interaction on energy spectra and *pn* correlations of the $J^\pi T = 1^+_1 0$, $3^+_1 0$, and $0^+_1 1$ states. The $1^+_1 0$ state has almost no energy gain of the spin-orbit interaction, whereas the $3^+_1 0$ state gains the spin-orbit interaction energy largely to come down to the ground state. We analyze the spin-orbit interaction dependence of the ^{10}B spectra and find that the ordering of the $3^+_1 0$ and $1^+_1 0$ states is sensitive to the spin-orbit interaction. We also apply a $2\alpha + pn$ model to discuss effects of the spin-orbit interaction on $T = 0$ and $T = 1$ *pn* pairs around the 2α core. In the spin-aligned $J^\pi T = 3^+0$ state, the spin-orbit interaction affects the $(ST) = (10)$ pair attractively and keeps the pair close to the core, whereas, in the 1^+0 state, it gives a minor effect to the $(ST) = (10)$ pair. In the 0^+1 state, the $(ST) = (01)$ pair is somewhat dissociated by the spin-orbit interaction.

DOI: 10.1103/PhysRevC.91.054323 PACS number(s): 21.10.−k, 21.30.Fe, 21.60.Gx, 27.20.+n

I. INTRODUCTION

In the progress of experimental research on proton-rich nuclei, the interest of proton and neutron (*pn*) pair correlations has been revived in recent years. In the study of *pn* pairing, the competition between isoscalar $T = 0$ pairing and isovector $T = 1$ pairing is one of the essential problems in $Z \sim N$ nuclei [1–10]. The nuclear interaction in a free space is more attractive in the $T = 0$ spin-triplet even (^{3}E) channel than in the $T = 1$ spin-singlet even (^{1}E) channel as known from the bound state, deuteron, formed by two nucleons in the ^{3}E channel. However, at the nuclear surface and in nuclear media, the competition between $T = 0$ and $T = 1$ *pn* pairs occurs. Because the ^{3}E interaction is stronger than the ^{1}E interaction, it is naively expected that the deuteronlike $T = 0$ pair is more favored than the $T = 1$ pair as seen in the ground state spin, $J^\pi T = 1^+0$, of ^{6}Li and ^{18}F. However, the $T = 1$ pair is often favored rather than the $T = 0$ pair in medium- and heavy-mass regions as seen in the ground state spins of $Z = N =$ odd nuclei because the spin-orbit mean potential favors the $T = 1$ pair [11]. Moreover, the spin-orbit potential favors a spin-aligned $T = 0$ *pn* pair [12–14]. These facts indicate that the spin-orbit interaction plays an important role in the competition between $T = 0$ and $T = 1$ *pn* pairs in nuclear systems.

Investigations of $Z = N =$ odd nuclei are helpful to understand features of *pn* pairs at the nuclear surface. Based on a three-body picture of a core nucleus with two valence nucleons, one can discuss the competition between $T = 0$ and $T = 1$ *pn* pairs from the ordering of $J^\pi T = 1^+0$ and 0^+1 states. For example, ^{6}Li and ^{18}F have the $J^\pi T = 1^+0$ ground states and the $J^\pi T = 0^+1$ excited states indicating that the $T = 0$ pair is favored rather than the $T = 1$ pair. However, in ^{42}Sc, the ground state is $J^\pi T = 0^+1$ because the $T = 1$ pair is favored by the spin-orbit potential at the surface of the ^{40}Ca core as discussed by Tanimura *et al.* based on a three-body model calculation [15].

In the previous paper [16], two of the authors, Kanada-En'yo and Kobayashi, discussed effects of the spin-orbit interaction on *pn* pairs at the surface of ^{16}O in ^{18}F based on an ^{16}O + *pn* model and found that the level structure of $J^\pi T = 1^+0$, 0^+1, and 3^+0 states is affected by the strength of the spin-orbit interaction. Namely, the spin-orbit interaction reduces the $T = 1$ pair energy in the 0^+1 state, and it largely contributes to the energy of a spin-aligned $T = 0$ *pn* pair attractively to lower the 3^+0 energy, whereas it gives a minor effect to the $T = 0$ pair energy in the 1^+0 state.

In ^{10}B, the ground state is the 3^+0 state and the first excited state is the 1^+0 state at $E_x = 0.72$ MeV. Based on a $2\alpha + pn$ picture, this fact indicates that ^{10}B is an interesting system in which the level inversion between the 1^+0 state having a $T = 0$ pair in an S wave (a pair moving in the total-angular-momentum $L = 0$ state around the core) and the 3^+0 state having a spin-aligned $T = 0$ pair [a pair moving in a total-angular-momentum $L = 2$ (D-wave) state around the core] occurs.

Since the 2000s *ab initio* calculations using realistic nuclear force have been achieved for $A \sim 10$ nuclei with such approaches as the Green's function Monte Carlo (GFMC) [17,18] and the no-core shell model (NCSM) [19,20]. The experimental low-lying spectra of ^{10}B were described well by the GFMC calculations with nuclear forces including the realistic two-nucleon (NN) forces and the pion-exchange-based three-nucleon (NNN) forces [21], which clearly showed the necessity of the NNN force to reproduce the experimental ordering of the 3^+0 and 1^+0 states in ^{10}B [17,18]. Also the NCSM calculations with effective interactions derived from the chiral NN and NNN nuclear forces [22–24] describe well the low-lying spectra of ^{10}B and show that the NNN force is essential to reproduce the 3^+0 and 1^+0 ordering [20]. Recently, Kohno pointed out that the NNN force provides an attractive contribution to the effective two-body spin-orbit interaction in a nuclear medium based on a G-matrix analysis [25].

Therefore, it is expected that the NNN force may also contribute to *pn* pairs in nuclei through the effective spin-orbit interaction.

In this paper, we investigate the structure of ^{10}B and clarify the effects of the spin-orbit interaction on $T = 0$ and $T = 1$ *pn* pairs based on the calculation of antisymmetrized molecular dynamics (AMD) [26–28] using phenomenological effective nuclear interactions. The AMD method is a model for structure studies and has been proved to be one of the successful methods for light nuclei, in particular, to describe cluster structures of ground and excited states. For instance, 2α cluster structures of neutron-rich Be isotopes are described systematically with the AMD calculations [26,29]. We calculate ^{10}B with the AMD method and find that a 2α cluster core is formed in ^{10}B. We discuss the role of the spin-orbit interaction in energy spectra and features of a *pn* pair around the 2α core in ^{10}B. Moreover, we associate a part of the effective two-body spin-orbit interaction with the NNN force based on the Kohno evaluation and discuss its effect on the ^{10}B energy spectra. We also discuss ^{6}Li spectra having a *pn* pair around an α core for comparison.

This paper is organized as follows. In Sec. II, we explain the formulation of the AMD method. In Sec. III, the calculated results for ^{10}B are shown. We discuss effects of the spin-orbit interaction on the ^{10}B energy spectra based on the AMD result in Sec. IV. In Sec. V, we perform an analysis using a $2\alpha + pn$ model to discuss the effects of the spin-orbit interaction on the *pn* pair around the 2α core. A summary is given in Sec. VI.

II. FORMULATION OF AMD AND EFFECTIVE NUCLEAR INTERACTIONS

A. AMD method

We apply the method of the variation after parity and total-angular-momentum projections of the AMD model (AMD+VAP) [30,31] to obtain A-nucleon wave functions for the ground and excited states of a nucleus with mass number A. We here briefly explain the formulation of the present AMD calculation.

An AMD wave function is given by a Slater determinant,

$$\Phi_{\rm AMD}(\mathbf{Z}) = \frac{1}{\sqrt{A!}}\mathcal{A}\{\varphi_1,\varphi_2,\ldots,\varphi_A\}, \tag{1}$$

where $\mathcal{A}$ is the antisymmetrizer, and the ith single-particle wave function is written by a product of spatial (ϕ_i), intrinsic spin (χ_i), and isospin (τ_i) wave functions as

$$\varphi_i = \phi_{\mathbf{X}_i}\chi_i\tau_i, \tag{2}$$

$$\phi_{\mathbf{X}_i}(\mathbf{r}_j) = \left(\frac{2\nu}{\pi}\right)^{4/3}\exp\left\{-\nu\left(\mathbf{r}_j - \frac{\mathbf{X}_i}{\sqrt{\nu}}\right)^2\right\}, \tag{3}$$

$$\chi_i = \left(\frac{1}{2}+\xi_i\right)\chi_\uparrow + \left(\frac{1}{2}-\xi_i\right)\chi_\downarrow, \tag{4}$$

where $\phi_{\mathbf{X}_i}$ and χ_i are spatial and spin functions, respectively, and τ_i is the isospin function fixed to be up (proton) or down (neutron). Accordingly, an AMD wave function is expressed by a set of variational parameters, $\mathbf{Z} \equiv \{\mathbf{X}_1,\mathbf{X}_2,\ldots,\mathbf{X}_A,\xi_1,\xi_2,\ldots,\xi_A\}$, which specify centroids of single-nucleon Gaussian wave packets and spin orientations for all nucleons.

The parameters $\mathbf{Z}$ are determined by the energy variation after parity and total-angular-momentum projections to obtain the optimized AMD wave function. Namely, in the AMD+VAP method, $\mathbf{X}_i$ and ξ_i $(i = 1 \sim A)$ for the lowest J^π state are determined so as to minimize the energy expectation value of the Hamiltonian, $\langle\Phi|H|\Phi\rangle/\langle\Phi|\Phi\rangle$, for the J^π eigenwave function projected from the AMD wave function; $\Phi = P^{J\pi}_{MK}\Phi_{\rm AMD}(\mathbf{Z})$. Here, $P^{J\pi}_{MK}$ is the parity and total-angular-momentum projection operator. For each J^π state, the optimum set $\mathbf{Z}^{(0)}_{J\pi}$ of parameters is obtained. After the VAP, to describe J^π_k states, we superpose the J^π-projected AMD wave functions expressed by the obtained parameter sets $\mathbf{Z}^{(0)}_{J'\pi'}$ for various $J'^{\pi'}$ as

$$\Psi_{J^\pi_k} = \sum_{J'^{\pi'},K} a_{J^\pi_k}(J'\pi';K)P^{J'\pi'}_{MK}\Phi_{\rm AMD}\big(\mathbf{Z}^{(0)}_{J'\pi'}\big), \tag{5}$$

where coefficients $a_{J^\pi_k}(J'\pi';K)$ are determined by diagonalizing the norm and Hamiltonian matrices. For $Z = N =$ odd nuclei, $T = 0$ and $T = 1$ projections are approximately done by using the proton-neutron exchanging operator $P_{p\leftrightarrow n}$ after the energy variation as

$$\Psi_{J^\pi_k} = \sum_{J'^{\pi'},K}\left\{a_{J^\pi_k}(J'\pi';K) + b_{J^\pi_k}(J'\pi';K)P_{p\leftrightarrow n}\right\} \times P^{J'\pi'}_{MK}\Phi_{\rm AMD}\big(\mathbf{Z}^{(0)}_{J'\pi'}\big), \tag{6}$$

where $a_{J^\pi_k}(J'\pi';K)$ and $b_{J^\pi_k}(J'\pi';K)$ are determined by the diagonalization. For $T = 0$ and $T = 1$ states, $a_{J^\pi_k}(J'\pi';K) \approx -b_{J^\pi_k}(J'\pi';K)$ and $a_{J^\pi_k}(J'\pi';K) \approx b_{J^\pi_k}(J'\pi';K)$ are obtained, respectively. In the present framework, we do not explicitly assume $a_{J^\pi_k}(J'\pi';K) = \pm b_{J^\pi_k}(J'\pi';K)$ because the isospin symmetry is slightly broken in the Hamiltonian because of the Coulomb force. However, the obtained $\Psi_{J^\pi_k}$ for J^π_k states of ^{10}B and ^{6}Li are found to be approximately T eigenstates and can be assigned to experimental $J^\pi T$ states.

For the width parameter ν of single-nucleon Gaussian wave packets, we choose $\nu = 0.235$ fm^{-2} which is the same value used for ^{10}Be and ^{11}B in Ref. [32] and was originally determined for ^{9}Be in Ref. [33].

In the AMD framework, the existence of clusters is not assumed *a priori* because Gaussian centroids $\mathbf{X}_i$ of all single-nucleon wave packets are independently treated as variational parameters. Nevertheless, if the system energetically favors a specific cluster structure, such a structure is obtained in the energy variation because the AMD model space contains wave functions for various cluster structures. Therefore, the AMD method is suitable to investigate whether the clusters are formed or not in the system.

Note that the AMD wave function is similar to the wave function used in fermionic molecular dynamics (FMD) calculations [34,35], though some differences exist in width parameters of single-nucleon Gaussian wave packets and the variational procedure. Another difference in the AMD and FMD calculations is effective nuclear interaction. In the AMD calculations, phenomenological effective interactions are usually used differently from the recent FMD calculations,

in which effective interactions constructed from the realistic nuclear force by means of the unitary correlation operator method are used [35].

B. Effective nuclear interactions

We use the finite-range central and spin-orbit interactions as effective two-body nuclear interactions,

$$v_{12}^{\rm eff} = v_c(r)(w + bP_\sigma - hP_\tau - mP_\sigma P_\tau) + v_{ls}(r)\frac{1+P_\sigma}{2}\frac{1+P_\sigma P_\tau}{2}\boldsymbol{l}\cdot\boldsymbol{s}, \quad (7)$$

where P_σ and P_τ are the spin and isospin exchange operators, r is the relative distance $r = |\boldsymbol{r}|$ for the relative coordinate $\boldsymbol{r} = \boldsymbol{r}_1 - \boldsymbol{r}_2$, $\boldsymbol{l}$ is the angular momentum for $\boldsymbol{r}$, and $\boldsymbol{s}$ is the sum of nucleon spins, $\boldsymbol{s} = \boldsymbol{s}_1 + \boldsymbol{s}_2$. We ignore the ^{3}E term of the spin-orbit interaction. In the present paper, we use the Volkov No. 2 central interaction [36],

$$v_c(r) = v_1 \exp\left[-\left(\frac{r}{a_1}\right)^2\right] + v_2 \exp\left[-\left(\frac{r}{a_2}\right)^2\right], \quad (8)$$

with $v_1 = -60.65$ MeV, $v_2 = 61.14$ MeV, $a_1 = 1.80$ fm, and $a_2 = 1.01$ fm, and the spin-orbit term of the Gaussian 3-range softcore force (G3RS) [37],

$$v_{ls}(r) = u_1 \exp\left[-\left(\frac{r}{b_1}\right)^2\right] + u_2 \exp\left[-\left(\frac{r}{b_2}\right)^2\right], \quad (9)$$

with $b_1 = 0.60$ fm and $b_2 = 0.447$ fm.

For the Volkov central interaction, we use the Wigner and Majorana parameters, $w = 0.40$ and $m = 0.60$, which reproduce the α-α scattering phase shift, and the Bartlett and Heisenberg parameters, $b = h = 0.125$, which reproduce the deuteron binding energy. The b and h are the parameters which can control the ratio f of the ^{3}E interaction to the ^{1}E interaction for the fixed $w + m$ value as $f = (w + m + b + h)/(w + m - b - h)$. The ratio is $f = 1.67$ for the present parametrization. Generally, in effective two-body central interactions for structure models, the ratio may change depending on nuclear systems because of medium effects and it is usually somewhat suppressed in nuclei. Therefore, b and h can be regarded as adjustable parameters in nuclei. In addition to the default parametrization $b = h = 0.125$, we also use a modified one, $b = h = 0.06$, which gives a smaller ratio $f = 1.27$ to fit the relative energy between $T = 0$ and $T = 1$ states in ^{10}B spectra.

For the strengths of the spin-orbit interaction, we take $u_{ls} = u_1 = -u_2$; u_{ls} is the strength parameter of the effective spin-orbit interaction and, in principle, it may depend on nuclear systems reflecting contributions from the three-body force and the tensor force as well as the original spin-orbit force in bare nuclear forces. It may also have structure model dependence and, therefore, is considered to be an adjustable parameter in model calculations. In the present paper, we use $u_{ls} = 1300$ MeV to reproduce the ls splitting between $3/2^-$ and $1/2^-$ states in ^{9}Be in the AMD+VAP calculation. We also use a slightly weaker strength $u_{ls} = 1000$ MeV to see the dependence of the energy spectra on the strength u_{ls} of the spin-orbit interaction. The strength of the effective spin-orbit interaction can be estimated by the Scheerbaum factor B_S [25,38] defined as

$$B_S = -\frac{2\pi}{q}\int_0^\infty drr^3 j_1(qr)v_{ls}(r), \quad (10)$$

with $q = 0.7$ fm^{-1}. Here j_l is the spherical Bessel function. For the G3RS spin-orbit interaction with $u_{ls} = 1300$ and 1000 MeV, B_S equals 103 and 79 MeV.

TABLE I. Adopted parameter sets of effective nuclear interactions. The Bartlett (b) and Heisenberg (h) parameters for the Volkov No. 2 central interaction and the strength parameter u_{ls} for the G3RS spin-orbit interaction. The Wigner and Majorana parameters are fixed to be $w = 0.4$ and $m = 0.60$ for all sets. The ratio of the ^{3}E to ^{1}E interactions, f, of the central interaction and the Scheerbaum factor B_S of the spin-orbit interaction are also shown.

	(A)	(B)	(A′)	(B′)
$b = h$	0.125	0.06	0.125	0.06
f	1.67	1.27	1.67	1.27
u_{ls} (MeV)	1300	1300	1000	1000
B_S (MeV)	103	103	79	79

In Table I, we list the adopted interaction parameter sets of effective nuclear interactions labeled (A) and (B) with the strength u_{ls}=1300 MeV and (Y′) and (B′) with u_{ls}=1000 MeV.

III. RESULTS

We calculate ^{10}B with the AMD+VAP method. The AMD wave functions for $J^\pi = 0^+, 1^+, 2^+, 3^+$, and 4^+ states are obtained by VAP. We superpose J^π-projected states of 10 basis wave functions (five are the obtained wave functions and five are the $P_{p\leftrightarrow n}$-projected wave functions) to get energy levels. We also apply the AMD+VAP method to ^{6}Li and ^{9}Be and calculate low-lying states, ^{6}Li($1^+, 2^+, 3^+, 0^+$) and ^{9}Be($1/2^-, 3/2^-, 5/2^-, 1/2^+, 3/2^+, 5/2^+$).

In Fig. 1, we show energy spectra of ^{6}Li and ^{9}Be obtained by the AMD+VAP calculation using the interaction parameter sets (A) and (B) compared with the experimental data. In the ^{6}Li spectra, the level spacing between $J^\pi = 1^+0$, 3^+0, and 2^+0 states is reproduced reasonably. The excitation energy of the 0^+1 state is overestimated in the result (A) and underestimated in the result (B). This means that a value of the ratio f in between $f = 1.67$ for (A) and $f = 1.27$ for (B) is reasonable to reproduce the ^{6}Li spectra. It may indicate that the effective ^{3}E interaction is slightly weaker in ^{6}Li than that in a deuteron. In the ^{9}Be spectra, the excitation energy of the $1/2^-$ state is reproduced by adjusting the spin-orbit strength u_{ls} as mentioned previously. Excitation energies of positive-parity states are somewhat overestimated, maybe because the present model space of AMD wave functions is not sufficient to describe well $K^\pi = 1/2^+$ band states, which are successfully described by molecular orbital models [33,39].

We show the calculated energy spectra of ^{10}B compared with the experimental data in Fig. 2. We also show the energy spectra of the NCSM calculation with the chiral NN+NNN force. Both results (A) and (B) in the present calculation reproduce the ordering of the 3_1^+0 and 1_1^+0 states in ^{10}B. Namely,

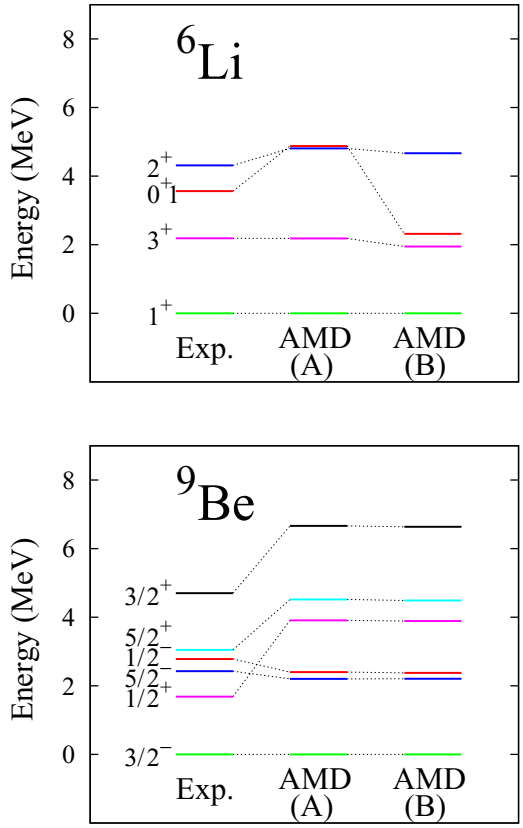

FIG. 1. (Color online) Energy spectra of ^{6}Li and ^{9}Be obtained by AMD+VAP using the interaction parameter sets (A) and (B) compared with the experimental spectra [40–42].

the $3^+_1 0$ is the ground state and the $1^+_1 0$ is the first excited state consistent with the experimental data and also with the NCSM calculation. The relative energy between the $3^+_1 0$ and $1^+_1 0$ states is sensitive to the strength of the effective spin-orbit interaction. More details of the dependence on the spin-orbit interaction and its relation to the NNN force are discussed later. The $0^+_1 1$ energy is largely overestimated in the result (A) and it is reasonably reproduced in the result (B), indicating that, in the present model, the smaller ratio $f \sim 1.27$ of the effective ^{3}E and ^{1}E interactions is more favorable for ^{10}B than $f \sim 1.67$ for a deuteron.

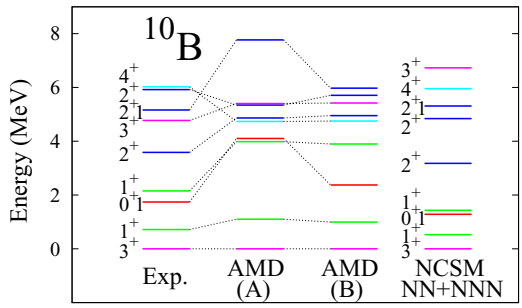

FIG. 2. (Color online) Energy spectra of ^{10}B. The theoretical result of AMD+VAP using the interaction parameter sets (A) and (B), the experimental data [40,42], and the NCSM calculation with the chiral NN+NNN force [20] are shown.

TABLE II. Properties of ^{6}Li, ^{9}Be, and ^{10}B. Theoretical values are calculated by AMD+VAP using the interactions (A) and (B). The experimental proton radii are derived from the charge radii in Ref. [43]. Other experimental data are taken from Refs. [40–42]. The values of the NCSM calculation with the chiral NN+NNN force from Ref. [20] are also shown.

		AMD+VAP		NCSM
	Expt.	(A)	(B)	NN+NNN
^{6}Li:$\lvert E(1^+_1 0)\rvert$	31.995	27.9	26.4	32.63
$r_p(1^+_1 0)$ (fm)	2.44(4)	2.21	2.21	
$Q(1^+_1 0)$ (e fm^2)	–0.0818(17)	0.09	0.08	–0.12(4)
$\mu(1^+_1 0)$ (μ_N)	0.822	0.88	0.88	0.836
$B(E2; 3^+_1 0 \to 1^+_1 0)$	10.7(8)	4.3	4.1	3.685
$B(E2; 2^+_1 0 \to 1^+_1 0)$	4.4(23)	5.5	5.2	3.847
$B(M1; 0^+_1 1 \to 1^+_1 0)$	15.4(3)	16.1	16.4	15.04(4)
^{9}Be:$\lvert E(3/2^-_1)\rvert$	58.164	53.0	53.0	
$r_p(3/2^-_1)$ (fm)	2.377(12)	2.42	2.42	
$Q(3/2^-_1)$ (e fm^2)	5.288(38)	5.2	5.2	
$\mu(3/2^-_1)$ (μ_N)	–1.1778(9)	–1.24	–1.24	
^{10}B:$\lvert E(3^+_1 0)\rvert$	64.751	58.7	57.7	64.78
$r_p(3^+_1 0)$ (fm)	2.28(5)	2.31	2.33	2.197
$Q(3^+_1 0)$ (e fm^2)	8.47(6)	7.95	8.2	6.327
$\mu(3^+_1 0)$ (μ_N)	1.8006	1.84	1.85	1.837
$\mu(1^+_1 0)$ (μ_N)	0.63(12)	0.86	0.84	
$B(E2; 1^+_1 0 \to 3^+_1 0)$	4.14(2)	4.2	3.6	3.05(62)
$B(E2; 1^+_2 0 \to 1^+_1 0)$	15.6(17)	10.2	10.1	
$B(E2; 1^+_2 0 \to 3^+_1 0)$	1.7(2)	0.9	1.3	0.50(50)
$B(E2; 2^+_1 0 \to 1^+_2 0)$	15.2(69)	2.7	4.3	
$B(E2; 2^+_1 0 \to 1^+_1 0)$	17.8(18)	7.9	7.6	
$B(E2; 2^+_1 0 \to 3^+_1 0)$	1.2(4)	1.1	0.9	
$B(E2; 3^+_2 0 \to 1^+_1 0)$	19.7(17)	7.7	8.3	
$B(M1; 0^+_1 1 \to 1^+_1 0)$	7.5(32)	13.5	14.7	
$B(M1; 1^+_2 0 \to 0^+_1 1)$	0.19(2)	0.0	0.0	
$B(M1; 2^+_1 1 \to 2^+_1 0)$	2.5(7)	3.7	3.9	
$B(M1; 2^+_1 1 \to 1^+_2 0)$	3.1(8)	2.8	2.7	
$B(M1; 2^+_1 1 \to 1^+_1 0)$	0.32(9)	0.2	0.4	

In Table II, properties of ^{6}Li, ^{9}Be, and ^{10}B are listed. The present results are compared with the experimental data and also theoretical values of the NCSM calculation with the chiral NN+NNN force [20]. Properties such as radii, moments, and transition strengths are reproduced reasonably by the present calculation.

IV. DISCUSSION

A. Dependence of energy spectra on spin-orbit interaction

To discuss the dependence of the energy spectra on the strength of the spin-orbit interaction, we compare the energy

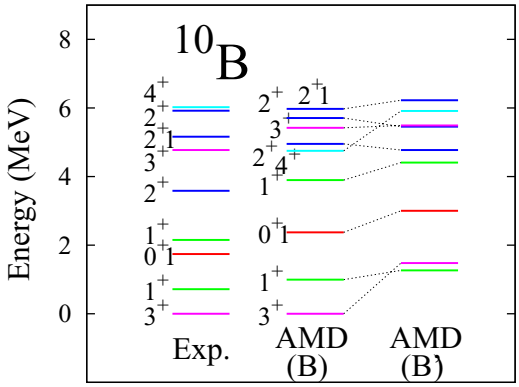

FIG. 3. (Color online) Energy spectra for ^{10}B calculated with AMD+VAP using interactions (B) and (B′). The experimental data are taken from Refs. [40,42].

spectra obtained using the interactions (B) with the default strength $u_{ls} = 1300$ MeV and those obtained using (B′) with a slightly weak spin-orbit interaction $u_{ls} = 1000$ MeV. We show ^{10}B spectra in Fig. 3. Energies relative to the $3^+_1 0$ energy of the result (B) are plotted. In the result (B′) with a weak spin-orbit interaction, the $1^+_1 0$ energy is lower than the $3^+_1 0$ state as expected from the *pn* pair picture that an $S = 1$ *pn* pair in the S wave is more favored than that in the D wave with no or a weak spin-orbit interaction. As a result, the interaction (B′) fails to describe the ordering of low-lying energy levels, i.e., the ground state spin, 3^+, of ^{10}B. However, in the result (B), the level inversion of the $3^+_1 0$ and $1^+_1 0$ states occurs consistently with the experimental data. The reason for the level inversion is that the spin-orbit interaction favors the spin-aligned $T = 0$ *pn* pair and lowers the $3^+_1 0$ state, whereas it gives almost no contribution to the energy of the $T = 0$ *pn* pair in the S wave in the $1^+_1 0$ state.

As for $T = 1$ states, the $0^+_1 1$ state somewhat gains the spin-orbit interaction energy because the spin-orbit interaction favors the $T = 1$ *pn* pair in the 0^+_1 state. In comparison of the results (B) and (B′), it is found that the energy gain for the 0^+_1 state is not as large as that for the $3^+_1 0$ state.

The present result indicates that the low-lying spectra of ^{10}B are sensitive to the spin-orbit interaction and the default spin-orbit strength which is phenomenologically adjusted to the *ls* splitting in ^{9}Be is found to be adequate to reproduce the 3^+0 and 1^+0 ordering. Let us remind the reader that, in the studies of ^{10}B with *ab initio* calculations using realistic nuclear forces, the 3^+0 and 1^+0 ordering can be described only when the NNN force is included. It is difficult to directly link the model calculation using phenomenological effective two-body interactions with the *ab initio* calculations using realistic nuclear forces. However, it is interesting to compare the present result with that of *ab initio* calculations considering a contribution of the NNN force to an effective two-body spin-orbit force in nuclei with the help of the Kohno G-matrix analysis as follows.

In general, a spin-orbit interaction in effective two-body nuclear interactions used for structure model calculations is an effective spin-orbit interaction in nuclei. It is usually phenomenologically adjusted to describe nuclear properties, and therefore, in principle, it may effectively reflect a contribution from the NNN force in addition to the original spin-orbit force in the bare NN forces. As Kohno pointed out, the NNN force contributes attractively to the effective two-body spin-orbit interaction in nuclear media [25]. In the G-matrix calculation of nuclear matters using the chiral NN and NN + NNN forces in Ref. [25], the contribution of the NNN force is evaluated to be $\Delta B_S = 20$–30 MeV of the Scheerbaum factor. For instance, in nuclear matter with the Fermi momentum $k_F = 1.35(1.07)$ fm^{-1}, the strength is estimated to be $B_S = 84.6(86.5)$ MeV for the chiral NN force and $B_S = 116.2(106.7)$ MeV for the chiral NN + NNN force.

In the present calculation, we use the phenomenological effective two-body central and spin-orbit interactions, which are adjusted so as to describe the α-α scattering and the *ls* splitting in ^{9}Be. Although the present interactions have no direct link to the bare nuclear forces, they may effectively reflect the contribution from the NNN force. Then, it is expected that a part of the two-body spin-orbit interaction in the present effective interactions can be interpreted as the contribution from the NNN force. With the help of the Kohno G-matrix analysis, we can roughly estimate the contribution of the NNN force in the present parametrization as the change $\Delta u_{ls} \sim 300$ MeV of the spin-orbit interaction strength which corresponds to the change $\Delta B_S = 24$ MeV of the Scheerbaum factor. Therefore, it is expected that the result (B′) with the weaker spin-orbit interaction by $\Delta u_{ls} \sim 300$ MeV than the default strength can be associated with the calculation without the NNN force contribution in the effective spin-orbit interaction. In Fig. 4, we show energy spectra of ^{10}B calculated with the interactions (B) and (B′), and those of the NCSM calculations with the chiral NN + NNN and the chiral NN forces. In each calculation, the energy of the $3^+_1 0$ state is set to be zero. As expected, differences in low-lying spectra between results (B) and (B′) in the present calculation correspond well to those of the NCSM results with and without the NNN force, meaning that the change $\Delta u_{ls} \sim 300$ MeV of the effective two-body spin-orbit interaction gives effects quite similar to the contribution of the NNN force on the low-lying spectra of ^{10}B. For instance, the $1^+_1 0$ state comes down to a lower energy region than the $3^+_1 0$ state in the result (B′) because of the reduction $\Delta u_{ls} \sim 300$ MeV consistently with the NCSM calculation without the NNN force. The excitation energy of the $0^+_1 1$ state is slightly decreased by the reduction $\Delta u_{ls} \sim 300$ MeV, which corresponds to the difference of the $0^+_1 1$ excitation energy between the NCSM calculation with the NNN force and that without the NNN force. This association of the present results (B) and (B′) with the NCSM calculations with and without the NNN force indicates that the part $\Delta u_{ls} \sim 300$ MeV of the two-body spin-orbit interaction in the present phenomenological effective interactions is interpreted as the contribution of the NNN force, which is essential to the level inversion between the $3^+_1 0$ and $1^+_1 0$ states in ^{10}B. We also show ^{6}Li spectra calculated with interactions (A) for the default spin-orbit interaction strength and (A′) for the reduced strength, compared with the chiral NN + NNN and NN NCSM calculations. Also for ^{6}Li, the change in the low-lying spectra by the reduction of $\Delta u_{ls} \sim 300$ MeV corresponds well to the difference between the NCSM calculations with and without the NNN force.

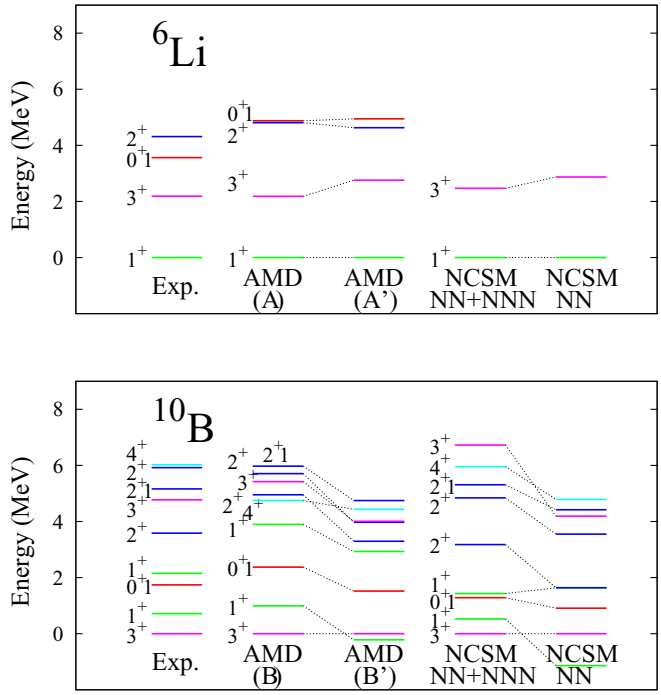

FIG. 4. (Color online) Dependence of the energy spectra on the strength $u_{\rm ls}$ of the spin-orbit interaction for ^{10}B and ^{6}Li calculated with AMD+VAP. Energy spectra of ^{10}B obtained using (B) with the default spin-orbit interaction $u_{\rm ls} = 1300$ MeV and (B′) with the weaker one, $u_{\rm ls} = 1000$ MeV, and those of ^{6}Li obtained using (A) with $u_{\rm ls} = 1300$ MeV and (A′) with $u_{\rm ls} = 1000$ MeV are shown as well as the experimental energy spectra. The NCSM calculation using the chiral nuclear forces with the NNN force (the chiral NN+NNN force) and without the NNN force (the chiral NN force) from Ref. [20] are also shown.

B. Structure of ^{10}B

We analyze ^{10}B wave functions obtained by AMD+VAP and find that the ground and excited states of ^{10}B are approximately understood by $T = 0$ of $T = 1$ *pn* pairs around the 2α core. In Table III, we show expectation values of the

TABLE III. Expectation values of harmonic oscillator quanta and those of the square spin and angular momentum for ^{10}B calculated with the interaction (A). For harmonic oscillator quanta, the minimum value $Q_{\rm min} = 6$ for the $0\hbar\omega$ configuration is subtracted, and values of $\Delta Q = \langle Q\rangle - Q_{\rm min}$ are listed.

^{10}B($J^\pi T$)	ΔQ	$\langle \boldsymbol{S}^2\rangle$	$\langle \boldsymbol{L}^2\rangle$
$3^+_1 0$	1.0	2.0	6.8
$1^+_1 0$	1.5	1.9	0.1
$0^+_1 1$	0.9	0.5	0.5
$1^+_2 0$	1.7	1.9	5.7
$2^+_1 0$	1.4	2.0	6.0
$3^+_2 0$	1.5	2.0	7.0
$2^+_1 1$	1.1	0.5	6.0
$2^+_2 0$	1.5	2.0	6.8
$4^+_1 0$	1.1	2.0	13.7

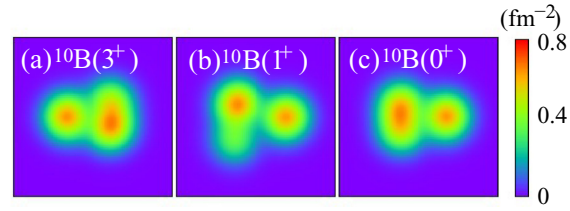

FIG. 5. (Color online) Distributions of matter densities of ^{10}B(3^+_1), ^{10}B(1^+_1), and ^{10}B($0^+_1, T = 1$) calculated with AMD+VAP using the interaction (A). Densities of intrinsic states are integrated with respect to the z axis and plotted on the x-y plane (the box size is 10 fm × 10 fm). Here, axes of the intrinsic frame are chosen as $\langle x^2\rangle \geqslant \langle y^2\rangle \geqslant \langle z^2\rangle$.

squared intrinsic spin, $\langle \boldsymbol{S}^2\rangle$, and those of the squared orbital angular momentum, $\langle \boldsymbol{L}^2\rangle$. We also show expectation values of the harmonic oscillator quanta, $\langle Q\rangle$, given by the creation and annihilation operators $Q = a^\dagger a$ of the harmonic oscillator for the width parameter $\nu = 0.235$ fm^{-2}. Since the 2α core gives no contribution to the total intrinsic spin, $\langle \boldsymbol{S}^2\rangle$ reflects mainly intrinsic spin configurations of two nucleons around the core. The calculated values of $\langle \boldsymbol{S}^2\rangle$ for $T = 0$ states are $\langle \boldsymbol{S}^2\rangle \approx 2$, indicating that two nucleons form a $(ST) = (10)$ pair, which is the same spin-isospin configuration as a deuteron. For $T = 1$ states, $\langle \boldsymbol{S}^2\rangle$ is approximately 0.5, meaning that the $T = 1$ *pn* pair has the dominant $(ST) = (01)$ component with a mixing of the $S = 1$ component. The $S = 1$ mixing in the $T = 1$ *pn* pair is nothing but the odd-parity mixing in the pair caused by the spin-orbit potential from the core as discussed in the previous paper for the *pn* pair around the ^{16}O core in ^{18}F. $\langle Q\rangle$ for the $1^+_1 0$ state is relatively large compared with those for the $3^+_1 0$ and $0^+_1 1$ states because the $1^+_1 0$ state has a spatially developed *pn* pair as well as the 2α clustering and contains higher shell components.

Figure 5 shows the matter density distribution of the intrinsic wave functions for the $3^+_1 0$, $1^+_1 0$, and $0^+_1 1$ states. The density of the single AMD wave function obtained by VAP for each J^π is shown. In the $3^+_1 0$ state, the $T = 0$ *pn* pair exists at the surface of an α cluster, whereas, in the $1^+_1 0$ state, it spatially develops. In the $0^+_1 1$ state, the $T = 1$ *pn* pair locates close to an α cluster. As mentioned previously, the $T = 0$ *pn* pair in the $3^+_1 0$ state and the $T = 1$ *pn* pair in the $0^+_1 1$ state are energetically favored by the spin-orbit potential from the core. To gain the spin-orbit potential, the *pn* pair remains at the surface close to the core in the $3^+_1 0$ and $0^+_1 1$ states. This is in contrast to the spatially developed $T = 0$ *pn* pair in the $1^+_1 0$ state, in which the spin-orbit interaction gives a minor contribution.

V. 2α + *pn* MODEL ANALYSIS OF *pn* PAIR

As discussed previously, the $3^+_1 0$ and $0^+_1 1$ states gain the spin-orbit interaction, whereas the $1^+_1 0$ state is not affected by the spin-orbit interaction. This result is understood by the effects of the spin-orbit potential on $T = 0$ and $T = 1$ *pn* pairs at the nuclear surface, which were discussed in the previous paper for ^{18}F based on the ^{16}O + *pn* model. To reveal the role of the spin-orbit interaction in the ^{10}B system, we here apply

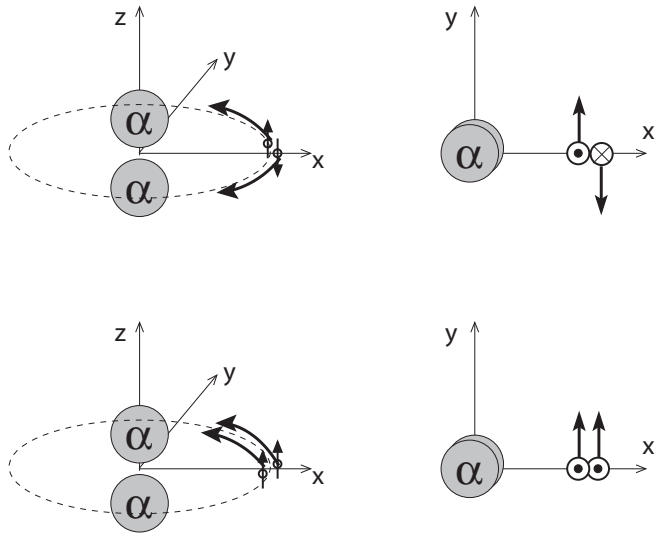

FIG. 6. Schematic figures for the $S_z = 0$ *pn* pair (top) and the $S_z = 1$ *pn* pair (bottom) around the 2α core in the $2\alpha + pn$ model.

a $2\alpha + pn$ model and investigate the effects of the spin-orbit interaction on the *pn* pair at the surface of the 2α core.

Let us consider a proton and a neutron at the surface of the 2α core. Because of the ^{3}E and ^{1}E interactions, they form $(ST) = (10)$ and $(ST) = (01)$ pairs. The former is the deuteronlike *pn* pair and the latter corresponds to the dineutron pair. For simplicity, we consider two nucleons with parallel intrinsic spins for the $T = 0$ pair and antiparallel intrinsic spins for the $T = 1$ pair around the 2α core as shown in Fig. 6. Here we take intrinsic spin orientations along the z axis for the α-α direction. Without the spin-orbit potential from the core, it is naively expected that $T = 0$ and $T = 1$ pairs move in the S wave ($L = 0$) around the 2α core in the lowest state to construct $J^\pi T = 1^+0$ and 0^+1 states. Due to the ^{3}E interaction being stronger than the ^{1}E interaction, the 1^+0 state is expected to be lower than the 0^+1 state. In the spin-orbit potential from the core, a spin-up nucleon at the surface is boosted to have finite momentum and a spin-down nucleon is boosted to the opposite direction. Consequently, for the $(ST) = (10)$ pair, the spin-orbit potential boosts two nucleons in the same direction and causes the orbital rotation of the pair, and therefore it favors the spin-aligned $J^\pi T = 3^+0$ state. For the $T = 1$ pair, the spin-orbit potential boosts two nucleons in the opposite direction. Due to the opposite boosting by the spin-orbit potential, the $T = 1$ pair is no longer the ideal $(ST) = (01)$ pair but it contains the odd-parity mixing, i.e., the mixing of the $S = 1$ component in the dominant $S = 0$ component as discussed in the previous paper.

To quantitatively discuss contributions of the spin-orbit interaction to $T = 0$ and $T = 1$ pairs in the $2\alpha + pn$ system, we introduce a $2\alpha + pn$ model as follows. The $2\alpha + pn$ wave function with antiparallel spins ($S_z = 0$) for the $T = 1$ *pn* pair is given as

$$\Phi^{S_z=0}_{2\alpha+pn} = \mathcal{A}\{\Phi_\alpha(\boldsymbol{R}_1)\Phi_\alpha(\boldsymbol{R}_2)\psi_{p\uparrow}(\boldsymbol{X}_1)\psi_{n\downarrow}(\boldsymbol{X}_2)\}, \quad (11)$$

$$\psi_{\tau\sigma}(\boldsymbol{X};\boldsymbol{r}) = \phi_{\boldsymbol{X}}(\boldsymbol{r})\chi_{\tau\sigma}, \quad (12)$$

where $\Phi_\alpha(\boldsymbol{R}_k)$ is the α cluster wave function written by the $(0s)^4$ harmonic oscillator configuration located at $\boldsymbol{R}_k$, and $\psi_{\tau\sigma}$ is the single-particle wave function for a valence nucleon assumed to be a localized Gaussian wave packet. Here we use labels $\tau = p,n$ and $\sigma = \uparrow,\downarrow$ for the isospin and intrinsic spin of the nucleon, respectively. We set two αs with the distance $d_{\alpha\alpha}$ parallel to the z axis as $\boldsymbol{R}_1 = -\boldsymbol{R}_2 = (0,0,d_{\alpha\alpha}/2)$, and the single-nucleon Gaussian wave packets for $p\uparrow$ and $n\downarrow$ at

$$\boldsymbol{X}_1 = (d_x, ik_y/2\nu, 0), \quad (13)$$

$$\boldsymbol{X}_2 = (d_x, -ik_y/2\nu, 0). \quad (14)$$

Here, parameters d_x and k_y stand for the mean positions and momenta of the Gaussian wave packets,

$$\langle\phi(\boldsymbol{X}_{1,2})|\hat{\boldsymbol{r}}|\phi(\boldsymbol{X}_{1,2})\rangle = (d_x,0,0), \quad (15)$$

$$\langle\phi(\boldsymbol{X}_1)|\hat{\boldsymbol{p}}|\phi(\boldsymbol{X}_1)\rangle = (0,\hbar k_y,0), \quad (16)$$

$$\langle\phi(\boldsymbol{X}_2)|\hat{\boldsymbol{p}}|\phi(\boldsymbol{X}_2)\rangle = (0,-\hbar k_y,0), \quad (17)$$

meaning that spin-up and- down nucleons are boosted to have finite momenta in the opposite direction (see top panels of Fig. 6). This parametrization is a kind of extension of the model for α cluster structures proposed by Itagaki *et al.* in Ref. [44]. Note that, in the $k_y \neq 0$ case, the *pn* pair contains the $S = 1$ component in addition to the dominant $S = 0$ component. The $2\alpha + pn$ wave function with parallel spins ($S_z = 1$) for the $T = 0$ *pn* pair is written as

$$\Phi^{S_z=1}_{2\alpha+pn} = \mathcal{A}\{\Phi_\alpha(\boldsymbol{R}_1)\Phi_\alpha(\boldsymbol{R}_2)\psi_{p\uparrow}(\boldsymbol{X}_1)\psi_{n\uparrow}(\boldsymbol{X}_2)\}, \quad (18)$$

with

$$\boldsymbol{X}_1 = (d_x, ik_y/2\nu, 0), \quad (19)$$

$$\boldsymbol{X}_2 = (d_x, ik_y/2\nu, 0), \quad (20)$$

where nucleons in the *pn* pair are boosted in the same direction (see bottom panels of Fig. 6).

For simplicity we fix the α-α distance as $d_{\alpha\alpha} = 3$ fm. The contribution from the center of mass motion is exactly removed by shifting Gaussian center positions as $\boldsymbol{R}_{1,2} \to \boldsymbol{R}_{1,2} - \boldsymbol{R}_G$ and $\boldsymbol{X}_{1,2} \to \boldsymbol{X}_{1,2} - \boldsymbol{R}_G$ with

$$\boldsymbol{R}_G = \frac{4(\boldsymbol{R}_1 + \boldsymbol{R}_2) + \boldsymbol{X}_1 + \boldsymbol{X}_2}{10}. \quad (21)$$

The J^π state projected from $\Phi^{S_z=\{0,1\}}_{2\alpha+pn}$ is given as

$$|J^\pi M\rangle_K = P^{J\pm}_{MK}\Phi^{S_z=\{0,1\}}_{2\alpha+pn}. \quad (22)$$

We calculate the energy expectation values of the 2α+*pn* wave functions using the interaction (A) and that without the spin-orbit interaction, and analyze energies of the T=1 and T=0 *pn* pairs in the $2\alpha + pn$ system.

We first discuss energies of $2\alpha + pn$ for the $k_y = 0$ case with no boosting, which corresponds to ideal $(ST) = (01)$ and $(ST) = (10)$ *pn* pairs. Figure 7 shows energies of the $J^\pi = 0^+$, 1^+, and 3^+ projected states, $P^{0+}_{M0}\Phi^{S_z=0}_{2\alpha+pn}$, $P^{1+}_{M1}\Phi^{S_z=1}_{2\alpha+pn}$, and $P^{3+}_{M3}\Phi^{S_z=1}_{2\alpha+pn}$, plotted as functions of the distance d_x of the pair position from the core. Here, $K = 0$, $K = 1$, and $K = 3$ are chosen for $J^\pi = 0^+$, 1^+, and 3^+ projections, respectively. Note that the $J^\pi = 0^+$ projected wave function is a $T = 1$ eigenstate and $\Phi^{S_z=1}_{2\alpha+pn}$ is a $T =$

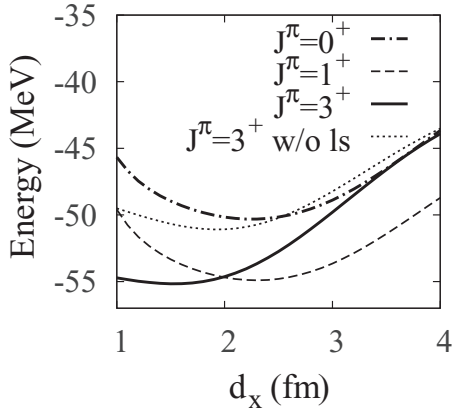

FIG. 7. d_x dependence of energy calculated with the $2\alpha + pn$ model. Energies of $J^\pi = 0^+$, 1^+, and 3^+ projected states for $k_y = 0$ are calculated using the interaction (A). The α-α distance is fixed to be $d_{\alpha\alpha} = 3$ fm. $S_z = 0$ is chosen for the 0^+ state, and $S_z = 1$ and $K = 1$ ($K = 3$) are chosen for the 1^+ (3^+) state. The 3^+ energy calculated without the spin-orbit interaction is also shown.

0 eigenstate. The $J^\pi = 0^+$ and 1^+ energy curves have minimums in the $d_x > 2$ fm region, indicating that the ideal $T = 1$ and $T = 0$ pn pairs develop spatially from the core. The spin-orbit interaction gives no contribution to the $(ST) = (01)$ pair in the 0^+ state or to the $(ST) = (10)$ pair in the 1^+ state. In the 3^+ energy curve obtained without the spin-orbit interaction, the optimum d_x at the energy minimum is slightly smaller than those for the 1^+ and 0^+ energy curves because of the relatively high centrifugal barrier. The 3^+ energy obtained with the spin-orbit interaction shows a large energy gain in the small d_x region. It indicates that the spin-aligned $T = 0$ pair is favored by the spin-orbit potential from the core, which keeps the pair close to the core.

Next we analyze the $k_y \neq 0$ case to discuss the contribution of the nucleon momenta. Figure 8 shows intrinsic energies of the $2\alpha + pn$ wave functions for $S_z = 0$ and $S_z = 1$ without the J^π projection and the $J^\pi = 0^+$ projected energy for $S_z = 0$. Energies are plotted as functions of the momentum k_y. For the $J^\pi = 0^+$ projected state, we also show $\langle \boldsymbol{S}^2 \rangle$, which indicates the $S = 1$ mixing (the odd-parity mixing) in the $S = 0$ component as a function of k_y. The pn pair position d_x is fixed to be $d_x = 2$ fm. In Figs. 8(a) and 8(c) for intrinsic energies, it is found that intrinsic states gain the spin-orbit interaction in the finite k_y region because of the boosting of nucleons in the opposite directions in the $S_z = 0$ pair and that in the same direction in the $S_z = 1$ pair. In the energy curve for the $(J^\pi = 0^+)$-projected state [see Fig. 8(b)], a further large energy gain of the spin-orbit interaction is found in the finite k_y region.

In Fig. 9, we show the 0^+ energy with and without the spin-orbit interaction plotted on the d_x-k_y plane. We also show the expectation value of the spin-orbit interaction of the 0^+ projected state. The energy surface obtained without the spin-orbit interaction shows the energy minimum at $d_x = 2.2$ fm on the $k_y = 0$ line [see Fig. 9(b)]. The contribution of the spin-orbit interaction is attractive in the finite k_y, in particular, in the small d_x region [see Fig. 9(c)], in which two nucleons

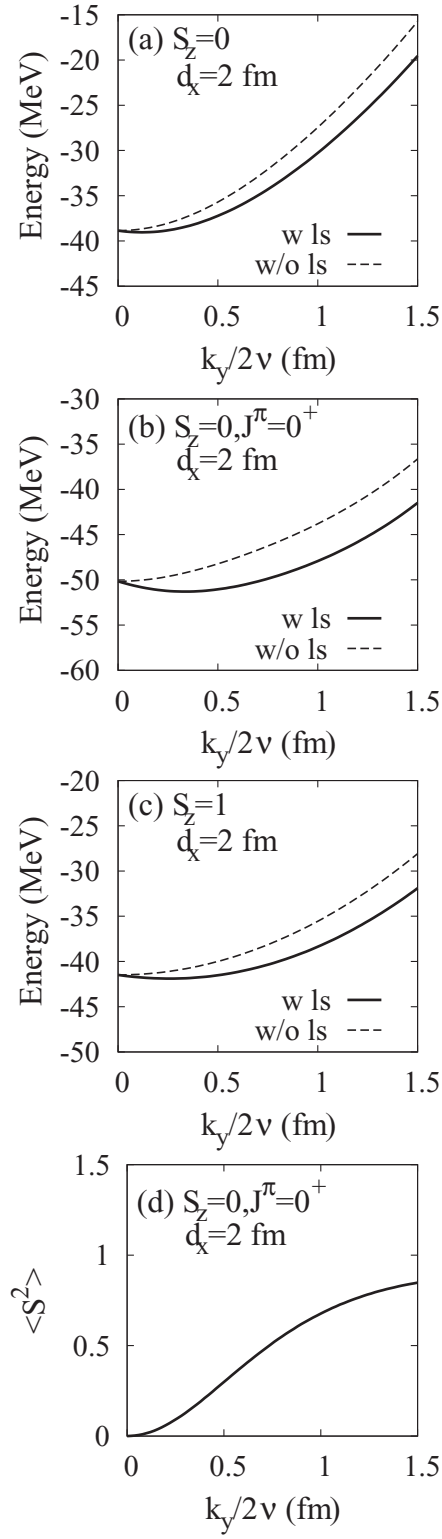

FIG. 8. Energies and $\langle S^2 \rangle$ calculated with the $2\alpha + pn$ model using the interaction (A). (a) Energy of the nonprojected state for the $S_z = 0$ pn pair, (b) that of the $J^\pi = 0^+$ projected state for the $S_z = 0$ pn pair, and (c) that of the nonprojected state for the $S_z = 1$ pn pair. The energies with and without the spin-orbit force are plotted as functions of k_y. $d_{\alpha\alpha} = 3$ fm and $d_x = 2$ fm are chosen. (d) The spin expectation value $\langle S^2 \rangle$ of the $J^\pi = 0^+$ projected state for the $S_z = 0$ pn pair.

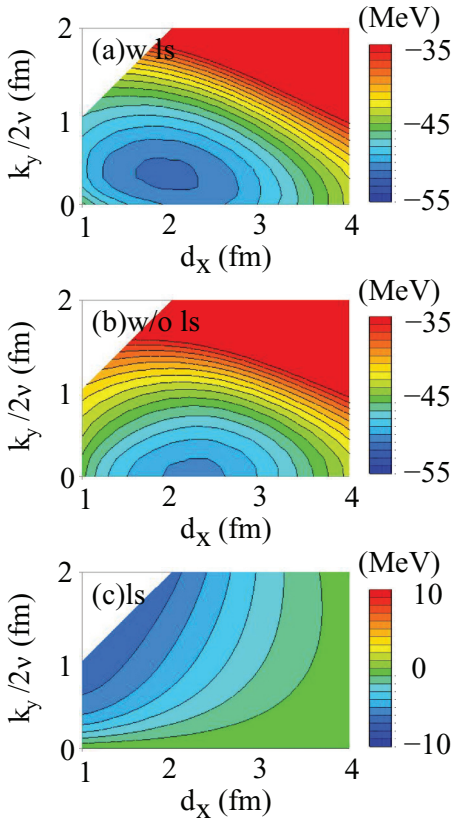

FIG. 9. (Color online) Energies of the $J^\pi = 0^+$ projected state for the $S_z = 0$ pn pair calculated with the $2\alpha + pn$ model using the interaction (A). (a) Energy with the spin-orbit interaction, (b) that without the spin-orbit interaction, and (c) the expectation value of the spin-orbit interaction.

in the $S_z = 0$ pair approximately occupy the single-particle $|\Omega| = |j_z| = 3/2$ orbits in the p shell. Consequently, the energy minimum shifts to the finite k_y and slightly smaller d_x region in the result with the spin-orbit interaction [see Fig. 9(a)]. This result indicates that the $(ST) = (01)$ pn pair in the 0^+ state is somewhat broken to contain the odd-parity mixing (the $S = 1$ mixing in the $S = 0$ component) by the spin-orbit potential at the surface from the core. Moreover, because of the spin-orbit potential, the spatial development of the pn pair is suppressed slightly.

VI. SUMMARY

We investigated the structures of positive-parity states of ^{10}B with AMD+VAP using the phenomenological effective two-body interactions. In the result, we found $2\alpha + pn$ structures in ^{10}B. We discuss effects of the spin-orbit force on the energy spectra and pn correlations in the $J^\pi T = 1^+_1 0, 3^+_1 0$, and $0^+_1 1$ states. The $1^+_1 0$ state is not affected by the spin-orbit interaction, whereas the $3^+_1 0$ state gains energy of the spin-orbit interaction largely, and the $0^+_1 1$ state also gains somewhat the energy of the spin-orbit interaction. When the default strength of the spin-orbit interaction is phenomenologically adjusted to the ^{9}Be spectra, the $3^+_1 0$ state comes down to the ground state, whereas, when a weaker spin-orbit interaction by $\Delta u_{ls} \sim 300$ MeV is used, the $3^+_1 0$ state becomes higher than the $1^+_1 0$ state. Thus, the spin-orbit interaction is found to be essential for the level ordering of the $3^+_1 0$ and $1^+_1 0$ states in ^{10}B. We showed that the change $\Delta u_{ls} \sim 300$ MeV of the spin-orbit interaction in the present effective two-body interactions gives effects quite similar to the contribution of the NNN force in the NCSM calculation on the low-lying spectra of ^{10}B and ^{6}Li. It may indicate that the part of the two-body spin-orbit interaction can be interpreted as the attractive contribution of the NNN force to the effective two-body spin-orbit interaction which was suggested by Kohno. We also applied the $2\alpha + pn$ model and discuss the effects of the spin-orbit interaction on the $T = 0$ and $T = 1$ pn pairs around the 2α core. In the spin-aligned $J^\pi T = 3^+0$ state, the spin-orbit interaction affects the $(ST) = (10)$ pair attractively and suppresses the spatial development of the pair, whereas, in the 1^+0 state, it has a minor effect on the $(ST) = (10)$ pair. The $(ST) = (01)$ pair in the 0^+1 state is somewhat dissociated to have the odd-parity mixing, i.e., the mixing of the $S = 1$ component by the spin-orbit interaction.

In the present calculation, we use the phenomenological effective two-body central and spin-orbit interactions, which are adjusted so as to describe the α-α scattering and the ls splitting in ^{9}Be. The present interactions have no direct link to the bare nuclear force although the contributions from the NNN force as well as the tensor force and also many-body effects in nuclear systems might be reflected in the effective interactions. In the present paper, we associate a contribution of the NNN force with a part of the effective two-body spin-orbit interaction, that is, $\Delta u_{ls} \sim 300$ MeV of the spin-orbit interaction strength following the Kohno evaluation from the G-matrix calculation for nuclear matter. However, it is difficult to prove one-to-one correspondence between terms of the present effective nuclear interactions and those of the bare nuclear forces. It is a remaining future problem to adopt more sophisticated effective interactions derived from bare nuclear forces to directly clarify the effects of the NNN force on the pn correlations in $Z = N =$ odd nuclei. It is also an important issue to study the effects of the NNN force on nuclear structures considering the link of the NNN force with the effective two-body spin-orbit interactions as done for nuclear radii by Nakada *et al.* [45].

ACKNOWLEDGMENTS

The computational calculations of this work were performed by using the supercomputers at YITP. This work was supported by Japan society of the promotion of science (JSPS) KAKENHI Grants No. 26400270 and No. 14J02221.

[1] A. L. Goodman, Adv. Nucl. Phys. **11**, 263 (1979).
[2] J. Engel, K. Langanke, and P. Vogel, Phys. Lett. B **389**, 211 (1996).
[3] W. Satula and R. Wyss, Phys. Lett. B **393**, 1 (1997).
[4] A. Poves and G. Martinez-Pinedo, Phys. Lett. B **430**, 203 (1998).
[5] A. L. Goodman, Phys. Rev. C **58**, R3051 (1998).

[6] K. Kaneko and M. Hasegawa, Phys. Rev. C **69**, 061302 (2004).
[7] S. Baroni, A. O. Macchiavelli, and A. Schwenk, Phys. Rev. C **81**, 064308 (2010).
[8] G. F. Bertsch and Y. Luo, Phys. Rev. C **81**, 064320 (2010).
[9] A. Gezerlis, G. F. Bertsch, and Y. L. Luo, Phys. Rev. Lett. **106**, 252502 (2011).
[10] H. Sagawa, Y. Tanimura, and K. Hagino, Phys. Rev. C **87**, 034310 (2013).
[11] A. O. Macchiavelli, P. Fallon, R. M. Clark, M. Cromaz, M. A. Deleplanque, R. M. Diamond, G. J. Lane, I. Y. Lee, F. S. Stephens, C. E. Svensson, K. Vetter, and D. Ward, Phys. Rev. C **61**, 041303 (2000).
[12] B. Cederwall *et al.*, Nature (London) **469**, 68 (2011).
[13] S. Zerguine and P. Van Isacker, Phys. Rev. C **83**, 064314 (2011).
[14] C. Qi, J. Blomqvist, T. Back, B. Cederwall, A. Johnson, R. J. Liotta, and R. Wyss, Phys. Rev. C **84**, 021301 (2011).
[15] Y. Tanimura, H. Sagawa, and K. Hagino, Prog. Theor. Exp. Phys. (2014) 053D02.
[16] Y. Kanada-En'yo and F. Kobayashi, Phys. Rev. C **90**, 054332 (2014).
[17] S. C. Pieper, K. Varga, and R. B. Wiringa, Phys. Rev. C **66**, 044310 (2002).
[18] R. B. Wiringa and S. C. Pieper, Phys. Rev. Lett. **89**, 182501 (2002).
[19] P. Navratil and W. E. Ormand, Phys. Rev. C **68**, 034305 (2003).
[20] P. Navratil, V. G. Gueorguiev, J. P. Vary, W. E. Ormand, and A. Nogga, Phys. Rev. Lett. **99**, 042501 (2007).
[21] S. C. Pieper, V. R. Pandharipande, R. B. Wiringa, and J. Carlson, Phys. Rev. C **64**, 014001 (2001).
[22] R. Machleidt and D. R. Entem, Phys. Rep. **503**, 1 (2011).
[23] E. Epelbaum, A. Nogga, W. Glöckle, H. Kamada, Ulf-G. Meißner, and H. Witala, Phys. Rev. C **66**, 064001 (2002).
[24] D. R. Entem and R. Machleidt, Phys. Rev. C **68**, 041001 (2003).
[25] M. Kohno, Phys. Rev. C **86**, 061301 (2012).
[26] Y. Kanada-En'yo, H. Horiuchi, and A. Ono, Phys. Rev. C **52**, 628 (1995).
[27] Y. Kanada-En'yo and H. Horiuchi, Phys. Rev. C **52**, 647 (1995).
[28] Y. Kanada-En'yo and H. Horiuchi, Suppl. Prog. Theor. Phys. **142**, 205 (2001).
[29] Y. Kanada-En'yo, M. Kimura, and A. Ono, Prog. Theor. Exp. Phys. (2012) 01A202.
[30] Y. Kanada-En'yo, Phys. Rev. Lett. **81**, 5291 (1998).
[31] Y. Kanada-En'yo and H. Horiuchi, Phys. Rev. C **68**, 014319 (2003).
[32] T. Suhara and Y. Kanada-En'yo, Prog. Theor. Phys. **123**, 303 (2010).
[33] S. Okabe and Y. Abe, Prog. Theor. Phys. **61**, 1049 (1979).
[34] H. Feldmeier, K. Bieler, and J. Schnack, Nucl. Phys. A **586**, 493 (1995).
[35] T. Neff and H. Feldmeier, Nucl. Phys. A **713**, 311 (2003).
[36] A. B. Volkov, Nucl. Phys. **74**, 33 (1965).
[37] N. Yamaguchi, T. Kasahara, S. Nagata, and Y. Akaishi, Prog. Theor. Phys. **62**, 1018 (1979); R. Tamagaki, *ibid.* **39**, 91 (1968).
[38] R. R. Scheerbaum, Nucl. Phys. A **257**, 77 (1976).
[39] M. Seya, M. Kohno, and S. Nagata, Prog. Theor. Phys. **65**, 204 (1981).
[40] F. Ajzenberg-Selove, Nucl. Phys. A **490**, 1 (1988).
[41] D. R. Tilley, C. M. Cheves, J. L. Godwin, G. M. Hale, H. M. Hofmann, J. H. Kelley, C. G. Sheu, and H. R. Weller, Nucl. Phys. A **708**, 3 (2002).
[42] D. R. Tilley, J. H. Kelley, J. L. Godwin, D. J. Millener, J. E. Purcell, C. G. Sheu, and H. R. Weller, Nucl. Phys. A **745**, 155 (2004).
[43] I. Angeli and K. P. Marinova, At. Data Nucl. Data Tables **99**, 69 (2013).
[44] N. Itagaki, H. Masui, M. Ito, and S. Aoyama, Phys. Rev. C **71**, 064307 (2005).
[45] H. Nakada and T. Inakura, Phys. Rev. C **91**, 021302 (2015).